WIND TUNNEL TESTING OF A 1/3RD SCALE MODEL GYROPLANE

F.N. Coton*, L. Smrcek*, Z. Pátek+

*Department of Aerospace Engineering,
University of Glasgow, U.K.
+ Aeronautical Research and Test Institute (VZLU),
Prague, Czech Republic

Abstract

This paper describes the wind tunnel testing of a scale model of a VPM M14 gyroplane in the 3m low speed wind tunnel at the Aeronautical Research and Test Institute (VZLU) Prague. These tests were conducted by the University of Glasgow as part of a U.K. Civil Aviation Authority funded research programme into gyroplane airworthiness and flight safety. The wind tunnel test programme had two distinct aims. The first was to provide basic aerodynamic data on the effects of configurational characteristics of a gyroplane with a view to assessing the degree to which specific design features such as cowlings and tailplanes are beneficial to gyroplane performance. Secondly, it was intended to provide aerodynamic data for input to mathematical models to validate parametric studies of static and dynamic stability carried out as part of the overall research programme. The results from the wind tunnel test programme show that the aerodynamic characteristics of the vehicle are generally benign although the cowling, which provides the pilot with protection from the elements, has a destablilsing influence under certain conditions.

Nomenclature

Cl	Rolling moment coefficient
Cm	Pitching moment coefficient
Cn	Yawing moment coefficient
Cx	Tangential Force coefficient
Cy	Sideforce coefficient
Cz	Normal force coefficient
R	Rotor radius
V_w	Wind speed
α	Angle of Attack
β	Sideslip angle
δ_r	Rudder deflection angle
ρ	air density

Introduction

The autogyro, or gyroplane, has been used for recreational and sport flying since before the Second World War. Despite this, however, gyroplanes have failed to establish a permanent foothold for either military or commercial applications. As a result, the machines have not been subject to the constant research and development focused on other flight vehicles. Consequently, the gyroplane of today is little different from its pre-war counterpart and, more importantly, lacks the technical back-up which would normally be attributable to a modern day aircraft.

The main body of research on gyroplane configurations dates from before 1940[1,9]. Although initial studies concentrated on the theoretical development of the vehicle, subsequent investigations addressed practical issues such as aerodynamics, performance and even rotor behaviour. Indeed, by the late nineteen thirties a sound basis existed for the future examination of the stability and control of these vehicles. Unfortunately, commercial and military interest in gyroplanes waned with the arrival of the helicopter in 1939 and, as a result, very little post-war research is documented. A study of gyroplane flight mechanics is, however, overdue in light of the accident rate suffered by the aircraft. In the U.K. alone, there were six fatal gyroplane accidents in the period 1989-91[10]. This viewpoint is reinforced by the continued popularity of gyroplanes with recreational flyers and also the potential which these machines have to provide low-cost flight data for rotorcraft modelling applications[11].

A major programme of research funded by the U.K. Civil Aviation Authority into gyroplane airworthiness and flight safety was initiated at the University of Glasgow in 1993[12]. The principal objectives of this study were to examine the stability and controllability of gyroplanes, to develop a computational tool which could be used to support studies into gyroplane stability and to support the development of a new airworthiness design standard in the UK; BCAR Section T [13]. To achieve these objectives, the overall programme was carried out in a phased manner as follows

Phase 1. Configuration of generic numeric models of rotorcraft to reproduce gyroplane behaviour and initial studies of gyroplane stability and control on this basis

Phase 2. Wind tunnel testing of a scale model gyroplane to examine basic aerodynamic characteristics of the flight vehicles and to provide input to the models developed under Phase 1. Additional studies of stability and control on the basis of the wind tunnel test results.

Phase 3. Flight testing of a comprehensively instrumented aircraft to allow validation of the computational models. This phase will also provide verification of assessments of the impact of operational and design parameters on airworthiness and flight safety made during Phases 1 and 2.

The detail of the numerical modelling procedures applied to the gyroplane have already been reported in Ref 12. This paper describes the wind tunnel tests carried out on a one third scale model gyroplane fuselage and presents the results of this phase of the work. In particular, the main aerodynamic characteristics of the gyroplane are highlighted and the influence of specific design features such as the cowling and vertical tail surfaces are also discussed.

Methods

Wind Tunnel Facility

All tests were conducted in the 3m Low Speed Wind Tunnel of the Aeronautical Research and Test Institute (VZLU) of Prague in the Czech Republic[14]. This institute has provided high quality wind tunnel facilities for the Czech aircraft industry for many years. The particular wind tunnel used in this study was an atmospheric open-section, closed return , Gottigen style tunnel with a maximum velocity of around 60m/s. Forces and moments were measured on a six component fully-automatic overhead gravitational balance which is accurate to between 0.01% and 0.05% full scale. The average turbulence intensity in the working section was 0.3%.

Wind Tunnel Model

The model used in this study was a powered, one-third scale model of a VPM-M14 gyroplane minus rotor as shown in Fig.1.

The basic model frame was constructed from metal box-section on which was mounted a water-cooled electric motor. This motor was connected by a toothed-belt to the propeller drive system. The removable tailplane assembly was fabricated in aluminium as were the representations of the aircraft wheels and wheel-covers. A scaled representation of the VPM-M14 cowling was made from glass fibre. In addition to the basic features of the aircraft, it was necessary to model the aerodynamic effect of the pilot. This was achieved by creating a representation of the pilot's upper-body which was mounted in an appropriate position on the model frame. The pilot's lower body was adequately represented by the motor which was positioned just above the main spar.

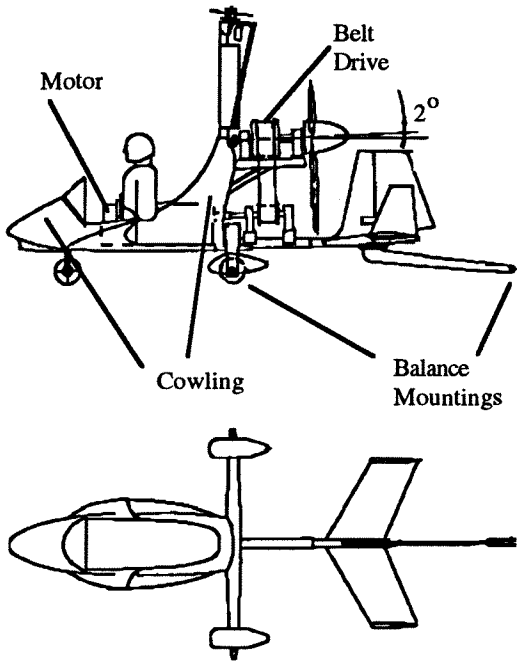

FIGURE 1 - Wind tunnel model

Test Set-up

The model was mounted in inverted mode on the wind tunnel balance via a series of connecting wires. Services to and from the motor were provided by a streamlined conduit which was located centrally above the model. This conduit, which was attached to the balance frame, not only provided a power supply for the model but also housed the water pipes necessary for the motor cooling system. The angle of attack and sideslip settings of the model were automatically adjusted using the balance control system. Rudder deflection was achieved manually.

The model was tested in both power on and power off modes. In the latter case, the propeller was removed from the model during testing. For powered tests, the model propeller operating conditions were appropriately matched to the cruise performance of the full scale VPM-M14 propulsion unit. This was achieved by matching the thrust coefficient of the model propeller to that of the full scale vehicle at an appropriate advance ratio. A stand alone calibration for the model propeller was available and an additional calibration involving measurements with the propeller attached to the gyroplane

fuselage was conducted. These data, together with drag measurements conducted on the fuselage in power off mode, allowed an appropriate blade pitch angle to be determined for the model propeller which simulated the required thrust and torque coefficients in cruise.

All tests were conducted at a test Reynolds number, based on the rotor radius, of 2.5 x10^6 which corresponds to a wind tunnel flow velocity of 31m/s. This test Reynolds number was approximately 40% of that of the full scale vehicle during cruise. The surfaces which are streamlined, such as the cowling and tail surfaces, all achieved test Reynolds numbers well in excess of the generally accepted threshold, Re = 250,000, below which undesirable low Reynolds number effects may be expected.

Test Series

The test programme involved tests on four gyroplane configurations, with the baseline being the cowling on, tail on configuration. The other configurations were produced by cowling on/off and horizontal tail on/off combinations. In addition, specific tests were conducted which involved extension of the tail boom and removal of the horizontal tail end-plates. In each case, however, force and moment coefficients were obtained for both power-on and power-off conditions.

In total, one hundred and fourteen data polars were measured covering the following parameter ranges

$$-40^o < \alpha < 40^o$$
$$-30^o < \beta < 30^o$$
$$-20^o < \delta_r < 20^o$$

Presentation of Coefficient Data

All force and moment coefficients presented in the following sections were measured with respect to the fuselage reference point and coordinate system shown in Fig. 2. The non-dimensional coefficients were calculated using the rotor radius as the basic characteristic length. Thus, for example, the normal force and pitching moment are given by

$$Z = \frac{1}{2} \rho V_w^2 \pi R^2 Cz$$

$$M = \frac{1}{2} \rho V_w^2 \pi R^3 Cm$$

respectively.

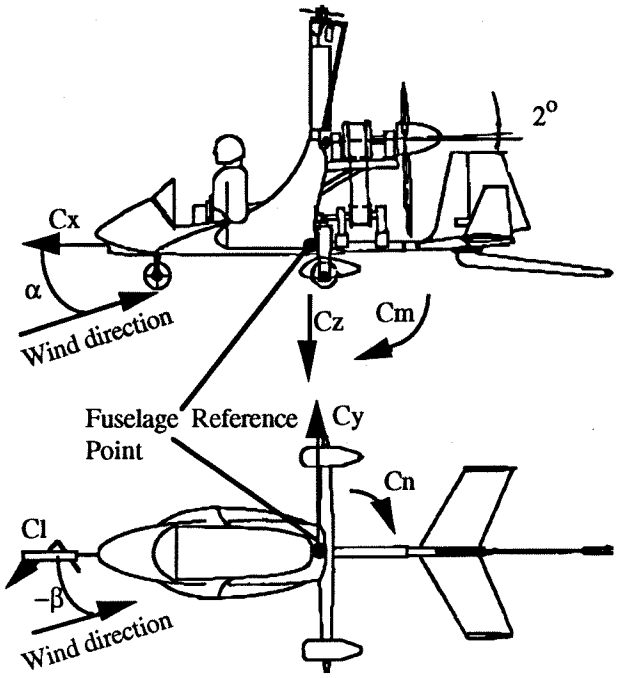

FIGURE 2 - Coordinate system

Discussion of Test Results

In this section, the main features of the results from the wind tunnel test programme are presented and analysed. Most of the data in this paper are those obtained for powered tests although there are selective comparisons with power off measurements. It should be noted that results identified as 'tail-off' relate to the removal of the horizontal tail surfaces and associated end plates only.

Normal Force Coefficient

Figure 3 presents the measured normal force coefficient variations at zero sideslip for each of the four configurations examined in the study. From this figure it is clear that, as may be expected, both the slope and magnitude of the normal force is most strongly influenced by the tailplane. It is also apparent that the influence of the cowling is generally small and, at positive incidence, acts in the same sense as the tailplane. This is presumably a result of the increased wetted area presented to the flow by the significant size of the cowling. At negative incidence, the cowling increasingly obstructs the propeller inflow, thus altering the nature of the slipstream behind the propeller. This produces different effects on Cz depending on whether the tail is on or off.

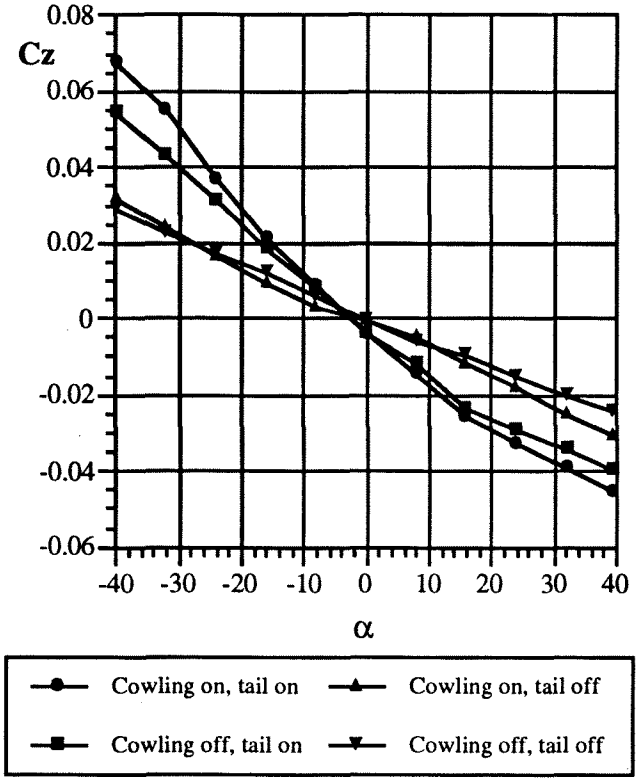

FIGURE 3 - Cz versus α for four gyroplane configurations. (β = 0)

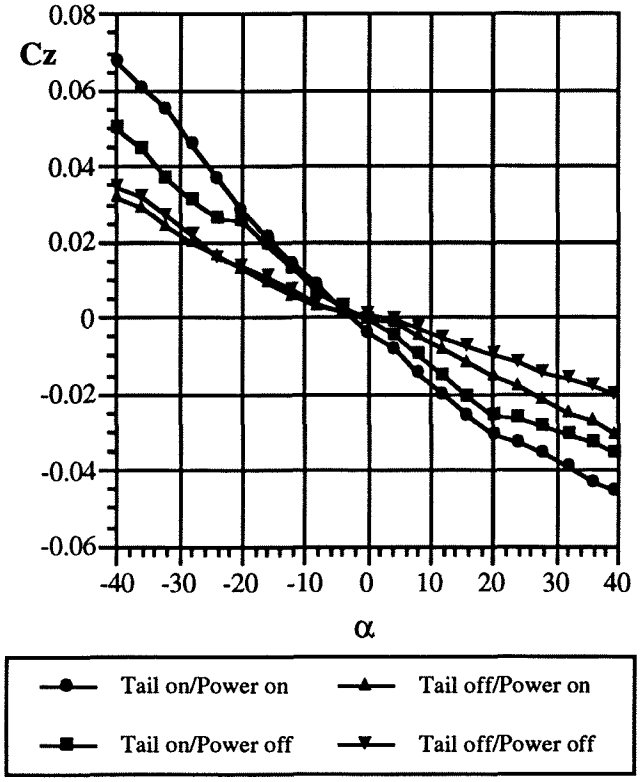

FIGURE 4 - The effect of power on Cz for tail-on and tail-off configurations (β=0)

Generally, the slopes of the Cz curves are almost linear, although there is a reduction in gradient at high positive incidence when the tailplane is on. This change in gradient appears to be due to tailplane stall as the tail moves away from the influence of the propeller slipstream. Conversely, at high negative incidence, the tail is fully enveloped by the propeller slipstream which, from simple momentum theory, has an average velocity three times the free stream. Thus, despite being subject to a reduced effective angle of attack, the tail generates more normal force because of the higher dynamic pressure it is subject to.

The full effect of the propeller may be observed in Fig. 4. where the normal force coefficient curves measured in power on and power off modes are compared for two of the test configurations. At positive incidence, the propeller inflow interacts with the freestream to modify the flow over the cowling thus increasing the normal force generated by it. On the other hand, the tail moves progressively out of the propeller slipstream and is observed to stall at the same incidence, regardless of power setting.

At negative incidence, the cowling presents less of a streamlined profile to the incident airflow and obstructs the flow into the propeller. Thus, as indicated above, the only significant effect of the propeller at negative incidence is to enhance the force produced by the tail.

The effect of sideslip angle on the normal force was found to be extremely small for incidence angles less that 20^{o}. At higher incidence, the angle at which tail stall occurred at both positive incidence was dependent on sideslip angle. This will be discussed in more detail when considering its effect on the pitching moment.

Tangential force

As may be anticipated, the primary influence on the tangential force is the thrust developed by the propeller since the propeller axis is only offset by 2^{o} from the coordinate thrust axis. Nevertheless, there are tangible effects of configuration which, in general, produce changes in thrust coefficient of around 4%. At high negative incidence, the change in tangential force due to configuration can be as much 20% of the propeller thrust. This is illustrated in Fig. 5. where the Cx versus a curves for the four configurations in power on mode are presented.

The most significant configurational effect is the additional thrust produced by the tail at negative incidence. In this case, the magnitude of the angle of attack experienced by the tail is less than the airframe incidence because the tail lies in the slipstream of the propeller. This prevents the tail from stalling and, because of the increased dynamic pressure in the slipstream, produces more thrust at high negative incidence.

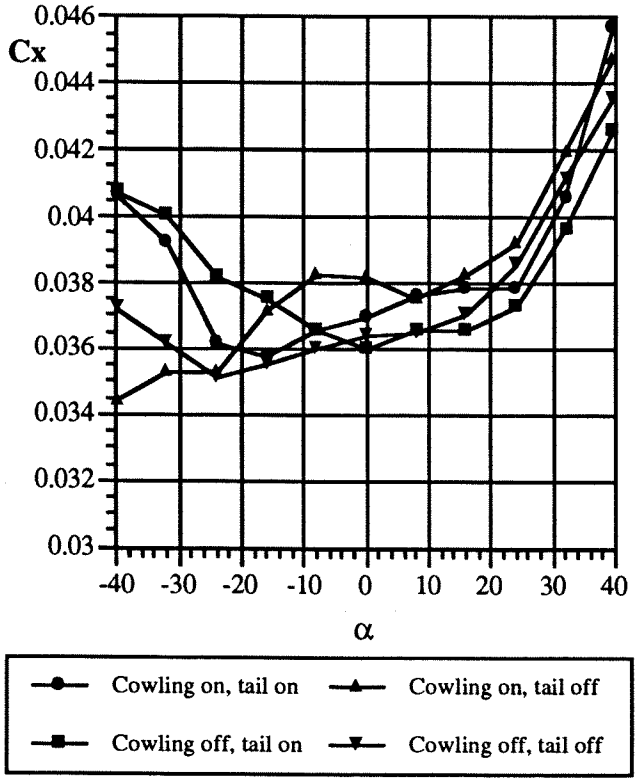

FIGURE 5 - Effect of gyroplane configuration on Cx (β=0)

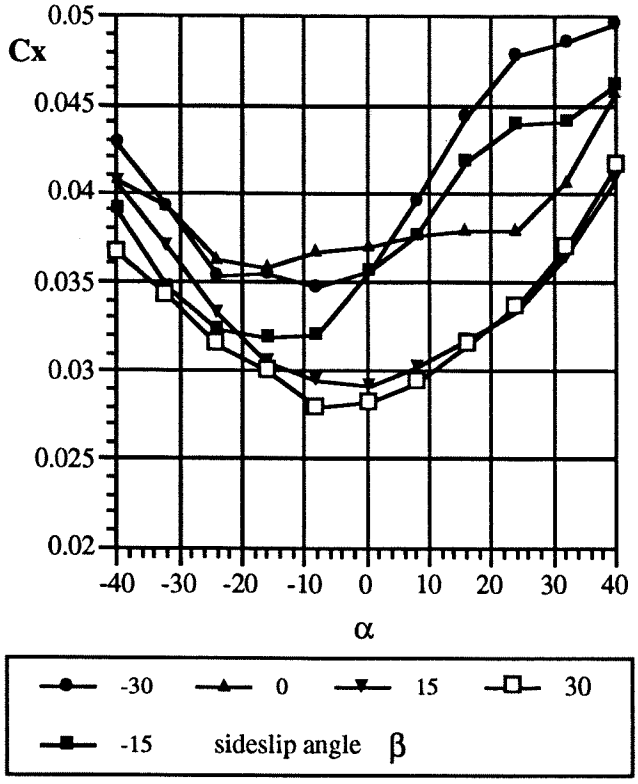

FIGURE 6 - Effect of sideslip angle on tangential force

Another interesting characteristic of the tail is apparent in the variation of tangential force with sideslip angle presented in Fig. 6. This time, however, the most significant effect is observed at positive incidence and is due to the vertical tail. The variation in Cx occurs because the resultant velocity and angle of attack experienced by the vertical tail, and hence the thrust developed by it, depends on the direction of the freestream and the axial and rotational velocities of the slipstream. At high incidence the variation in onset conditions is particularly large because the strong vortex structures produced by the propeller tips are convected over the main body of the vertical tail surface.

Sideforce coefficient

As shown in Fig. 7, the variation of sideforce with sideslip angle was found to almost linear in the range $-15^{o} < \beta < 15^{o}$. In the case of the cowling on, tail on configuration, tests were conducted up to sideslip angles of 30^{o} and , even there, little variation in gradient was found. The results were also relatively insensitive to model configuration and incidence setting with the principal influence being the vertical tail. It is, however, pertinent to note that a marginal increase in side force is produced when the horizontal tail is on. This is attributable to the increased side area presented by the vertical end-plates.

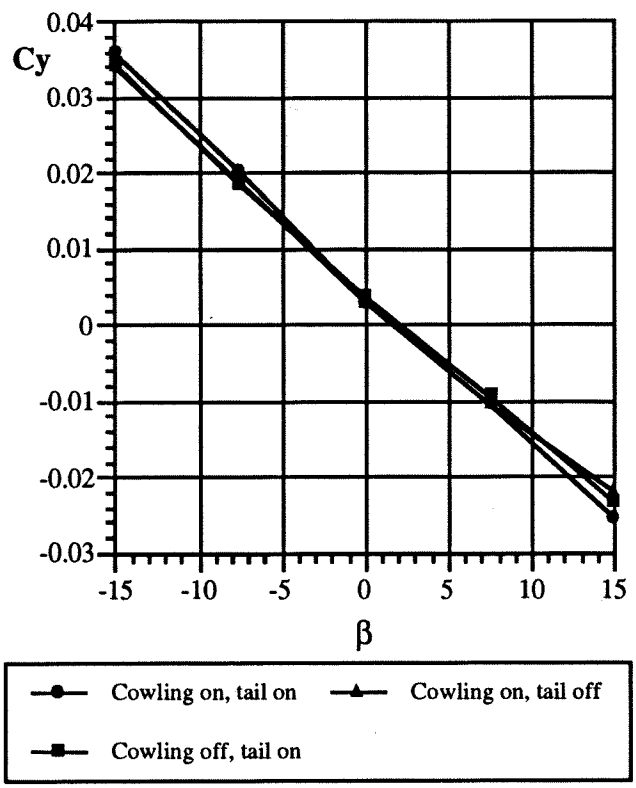

FIGURE 7 - Variation of sideforce with sideslip angle ($\alpha = 0$)

Pitching Moment Coefficient

The basic effects of configuration on the pitching moment are shown in Fig. 8. As may be expected, the horizontal tail acts to stabilise the flight vehicle and is effective up to its stalling incidence of around 20^{o}. At negative incidence, the effects discussed earlier, in connection with the normal force, come into play and tail stall is avoided.

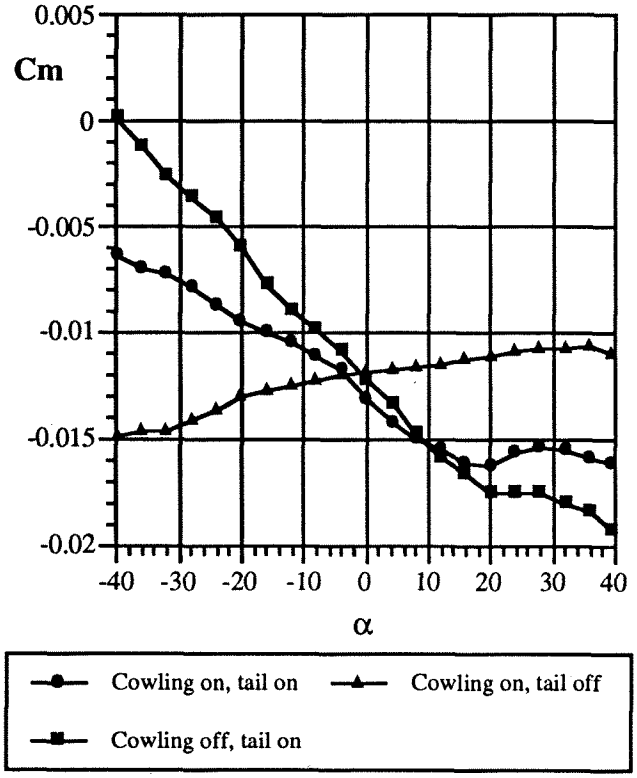

FIGURE 8 - Effect of configuration on Cm ($\beta = 0$)

Perhaps the most significant feature of the figure, however, is the strong destabilising effect of the cowling. With the tail on, the effect of the cowling is to reduce the gradient of the Cm curve by almost half. Without the tail, the cowling on configuration is statically unstable throughout the incidence range. This result is not surprising given the large wetted area presented by the cowling and its position ahead of the fuselage reference point. Nevertheless, the magnitude of the destabilising effect is substantial and has design implications.

Another interesting feature of the pitching moment behaviour is the extent to which it is influenced by power setting. In Fig. 9, results from the baseline configuration in power-on and power-off modes are compared. Clearly, the pitching moment produced by the propeller dominates the magnitude of the difference between the two curves. More subtle, however, is the effect produced by the tail at negative incidence as it enters the propeller slipstream. This increases the moment produced by the tail because of the effects of increased dynamic pressure and flow angularity, discussed in relation to the normal force. Generally, the net effect of the propwash with the tail is to produce a more linear Cm variation over the entire incidence range, thus enhancing stability.

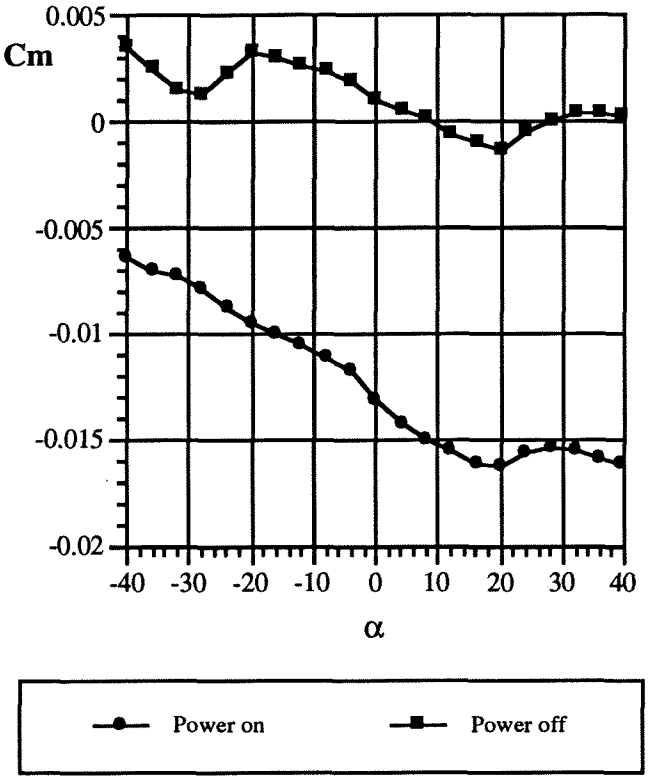

FIGURE 9 - Effect of power on Cm ($\beta = 0$)

The influence which the propeller slipstream/tail interaction has on the pitching moment was also found to vary with sideslip angle. This variation is complex and results from two distinct aspects of the interaction. The first is the effect of the axial velocity component of the propeller slipstream which, at moderate incidence washes over the horizontal tail, thus enhancing the lift produced by it. This results in a nose down pitching moment which reduces with increasing yaw magnitude and is illustrated in Fig. 10 where the pitching moment characteristics of the baseline configuration are presented for five sideslip angles.

A secondary effect on the tail results from the direction of rotation of the propeller slipstream. This can have a significant effect on both the direction and magnitude of the flow over the tail and, consequently, either moderates or enhances the effect of the increase in axial velocity in the slipstream. For this particular vehicle, the sense of rotation of the propeller is such that the tail experiences net downwash at positive yaw angles thus, generally, increasing the pitching moment.

Despite these effects, the sideslip angle produces only a small variation in the gradient of the Cm curves in the range $-20 < \alpha < 20$. Outside of this incidence range,

the stalling characteristics of the tail become significant and are seen to be strongly influenced by the propeller slipstream. The manner of this interaction is strongly three-dimensional but appears to be dominated, at negative incidence, by the enhanced axial velocity in the propeller slipstream. The most obvious effect of this is the prevention of stall when the gyroplane is head-on to the flow.

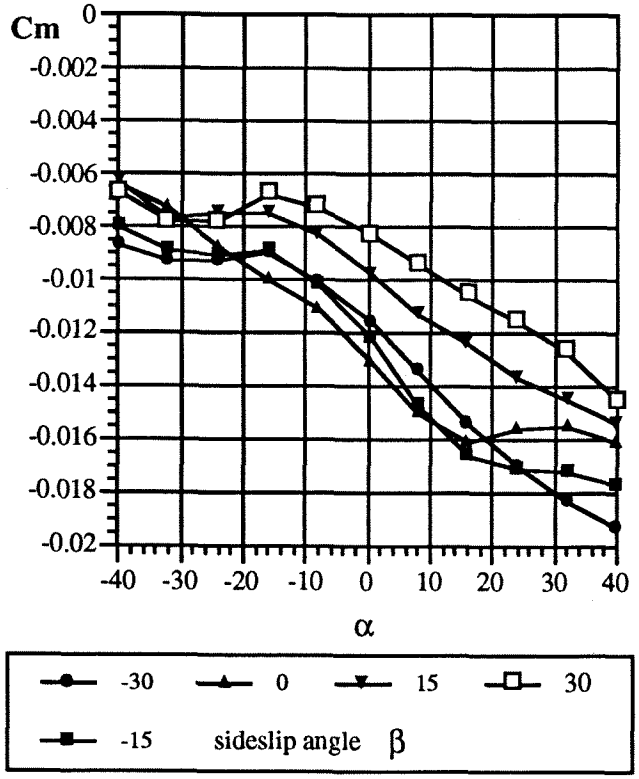

FIGURE 10 - Effect of sideslip angle on Cm

At positive incidence, the propeller slipstream lies above the tail and, consequently, its sense of rotation becomes a more significant factor. This is apparent in the delayed stall due to downwash at positive sideslip angles. One interesting anomaly appears to occur at -30° of sideslip where tail stall is not experienced. The reasons for this are unclear but may be due to additional effects such as wake skew or interaction of the slipstream with the vertical tail.

Rolling Moment Coefficient

The rolling moment produced by the gyroplane was found to be virtually insensitive to configuration and linear with respect to sideslip angle over the full test range. Similarly, the incidence setting also had little effect on the rolling moment.

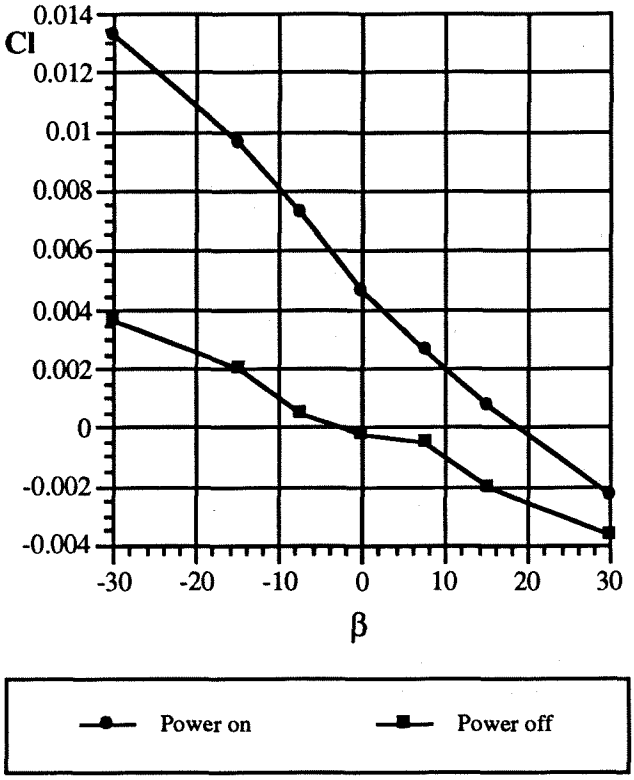

FIGURE 11 - Effect of power on Cl (α=0)

The main influence on the rolling moment was found to be the power setting. This is shown in Fig. 11 where the variations of rolling moment with sideslip are shown for the baseline configuration at zero incidence in power on and power off modes. For the head-on case, the magnitude of the rolling moment is increased with the power on as a consequence of the sideforce produced at the tail by the rotation of the propeller slipstream. This difference is, however, not constant and becomes much greater at high negative sideslip angles when the sideforce produced by the propeller wake becomes more aligned with the freestream.

Yawing Moment Coefficient

The influence of gyroplane configuration on the variation of yawing moment with sideslip angle is shown in Fig. 12. Clearly, the most stable characteristic is obtained with the horizontal tail on and the cowling removed. It is pertinent to note that the horizontal tail has large end-plates which, as discussed previously, contribute to the sideforce and hence the yawing moment. In fact, from the figure, it may be deduced that the effect of these surfaces almost totally offsets the destabilising influence of the cowling.

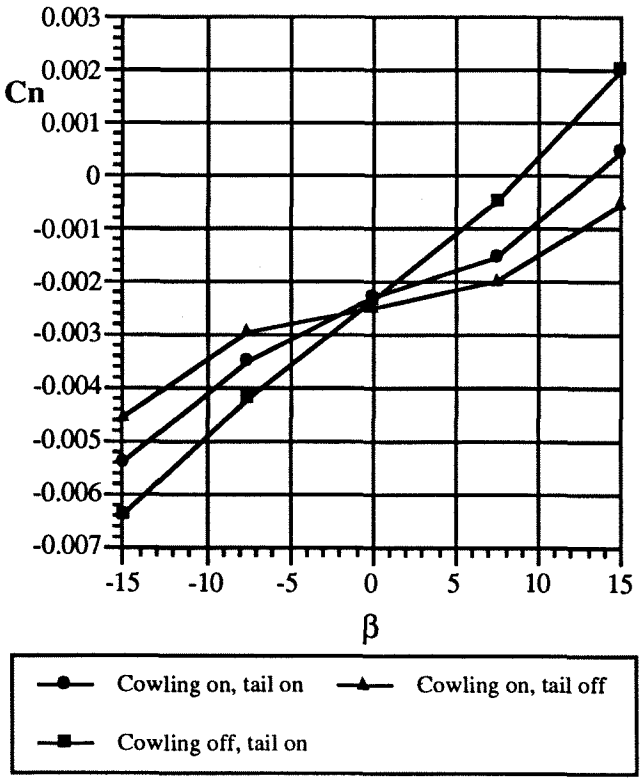

FIGURE 12 - Effect of configuration on Cn (α=0)

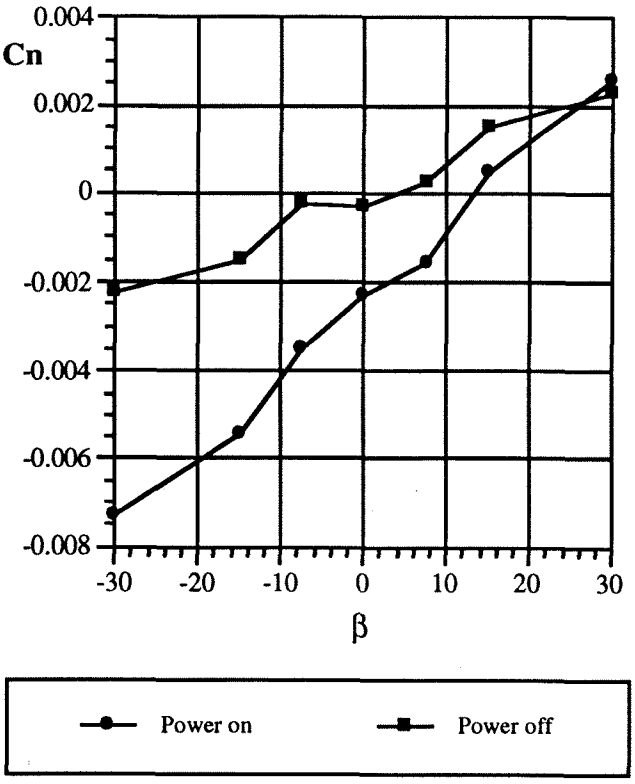

FIGURE 13 - Effect of power on Cn (α=0)

As may be expected, the yawing moment curve is strongly influenced by the power setting as shown in Fig 13. This is due to two particular effects. The first of these is the restoring torque produced by the propeller when it is offset from the freestream direction. This always provides a stabilising influence and, thus, has the effect of increasing the gradient of the curve. The second effect is the increase in sideforce produced at the tail because of the rotation of the propeller slipstream. This additional force always acts in the same direction and so gives a near constant offset to the curve. For this particular vehicle, the additional sideforce at the tail acts to reduce the yawing moment.

Rudder Effectiveness

The most significant effects of the rudder are on the side force and yawing moments. It was found that the rudder effect on both side force and yawing moment was almost linear at a given α regardless of power setting. This is illustrated in Fig. 14 where effect of rudder setting on Cn at zero incidence and sideslip is compared for power-on and power-off modes. It should be noted that in power-off mode, data were only measured for negative δ_r and at δ_r = 20°. Intermediate points are, therefore, interpolated for illustrative purposes.

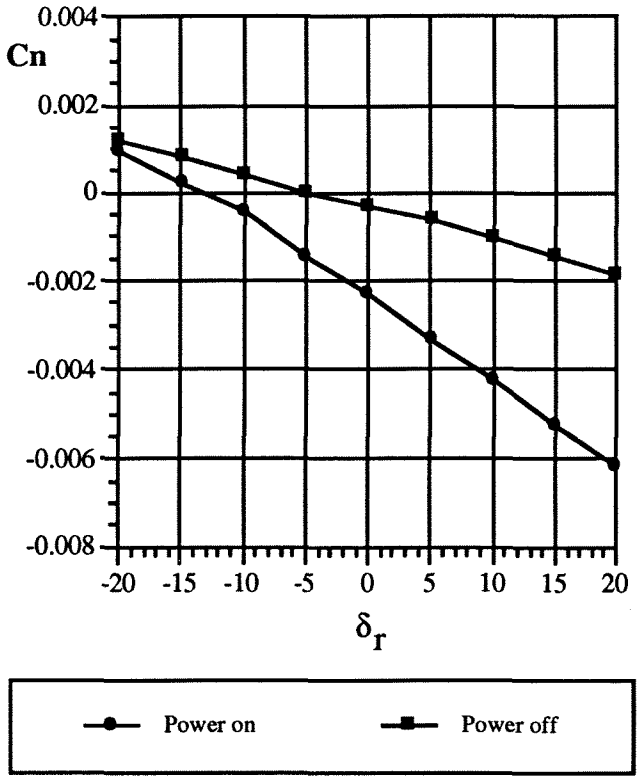

FIGURE 14 - Effect of power setting on rudder effectiveness ($\alpha = 0, \beta = 0$)

It may be observed that the effect of power is to substantially increase the gradient of the yawing moment

curve. As discussed previously, both the rotational and increased axial velocities, produced by the propeller, influence the performance of the vertical tail surfaces. The net result of power in this particular case is to almost double the gradient of the curve and, hence, the rudder effectiveness.

As in the case of the vertical tail, the enhanced performance of the rudder due to the propwash diminishes as the angle of attack of the gyroplane increases and the tail moves into clear air. In fact, regardless of power setting, the rudder effectiveness reduces at high α because of the strongly three dimensional flow around the tail surfaces.

The only other significant effect of the rudder arises from the displacement of its centre of pressure from the fuselage reference point. This produces a slight rolling moment when the rudder is deflected.

Concluding Remarks

The aerodynamic characteristics of the gyroplane configurations considered in this study are generally benign. It is, however, pertinent to note that there are several effects associated with the cowling which are detrimental to stability. Although the cowling on the VPM-M14 is particularly large, it is likely that any 'open' cowling design will be subject to similar effects in the longitudinal mode. Additionally, the length of the VPM cowling is substantial; extending from well in front of the pilot up to the rotor support column. The increased wetted area which this presents to the onset flow in sideslip acts so as to oppose the stabilising effect of the tail. The tail itself benefits from the additional sideforce produced by the endplates on the horizontal surfaces.

Acknowledgements

This work was supported by the UK Civil Aviation Authority under Contract 7D/S/1125 "Aerodynamics of Gyroplanes".

The authors also wish to acknowledge the contribution to the project of Prof. R. Galbraith and Dr. S. Houston of Glasgow University and Mr. M. Holl of VZLU.

References

1. Glauert, H., 'A general theory of the Autogyro', Aeronautical Research Committee, Reports and Memorandum No. 1111, 1926

2. Lock, C.N.H., 'Further development of autogyro theory parts I and II', Aeronautical Research Committee, Reports and Memorandum No. 1127, 1927

3. Glauert, H., 'Lift and torque of an autogyro on the ground', Aeronautical Research Committee, Reports and Memorandum No. 1131, 1927

4. Lock, C.N.H. and Townend, H.C.H., 'Wind tunnel experiments on a model autogyro at small angles of incidence', Aeronautical Research Committee, Reports and Memorandum No. 1154, 1927

5. Glauert, H., Lock, C.N.H., 'A summary of the experimental and theoretical investigations of the characteristics of an autogyro', Aeronautical Research Committee, Reports and Memorandum No. 1162, 1928

6. Wheatly, J.B., 'Wing pressure distribution and rotor blade motion of an autogyro as determined in flight', NACA TR 475, 1933

7. Wheatly, J.B., An aerodynamic analysis of the autogyro rotor with a comparison between calculated and experimental results', NACA TR 487, 1934

8. Wheatly, J.B., Hood, M.J., 'Full-scale wind tunnel tests of a PCA-2 autogyro rotor', NACA TR 515, 1935

9. Wheatly, J.B., 'An analytical and experimental study of the effect of periodic blade twist on the thrust, torque and flapping motion of an autogyro rotor', NACA TR 591, 1937

10. Anon., 'Airworthiness review of Air Command gyroplanes', U.K. Air Accidents Investigation Branch Report, 1991

11. McKillip, R.M., Chih, M.H., 'Instrumented blade experiments using a light autogyro', 16th European Rotorcraft Forum, Glasgow, 1990

12. Houston, S.S., Thomson, D.G., 'A study of gyroplane flight dynamics', 21st European Rotorcraft Forum, St. Petersburg, Russia, 1995

13. Anon, 'British Civil Airworthiness Requirements Section T: Light Gyroplanes', CAP 643, 1995

14. Soucek, T., Hanzl, M., 'Wind tunnel measurement of the autogyro model', VZLU Test Report Z-3545/94, 1994